Steady buoyant droplets with circulation

Shin-Shin Kao[a)]
Department of Mathematics, Chung-Yuan Christian University, Chung-Li, Taiwan

Russel E. Caflisch[b)]
Department of Mathematics, University of California at Los Angeles, Los Angeles, California 90095-1555

(Received 1 August 1996; accepted 22 April 1998)

Numerical solutions are presented for the steady flow corresponding to a two-dimensional moving droplet with circulation. Differences in the density of the droplet and surrounding fluid result in a buoyancy force which is balanced by a lift force due to the Magnus effect. The droplet is assumed to have constant vorticity in its interior, and its boundary may be a vortex sheet, as in a Prandtl–Batchelor flow. Only symmetric solutions are calculated. For Atwood number $A=0$ (no density difference) the droplet is a circle. As the Atwood number is increased, the droplet shape begins to resemble a circular cap with a dimpled base. There is a critical Atwood number $A_{\lim}$ at which the droplet develops two corners. For $0\leqslant A<A_{\lim}$, the solution is smooth; while for $A_{\lim}<A$, we do not find a solution. © *1998 American Institute of Physics.* [S1070-6631(98)02908-0]

I. INTRODUCTION

A 2-D fluid droplet of density ρ_1 surrounded by an unbounded fluid of different density ρ_2 experiences a buoyancy force $\mathbf{F}_g=-g(\rho_1-\rho_2)a\hat{\mathbf{y}}$ in which a is the area of the droplet. One possibility for balancing this buoyancy force is through the lift of the Magnus effect. If the droplet is moving at speed U in the x direction and has circulation Γ and if the ambient fluid is irrotational, then this lift force is $\mathbf{F}_l=-\Gamma U\rho_2\hat{\mathbf{y}}$. Thus there is a balance between these two forces if

$$\Gamma U=-ga(\rho_1-\rho_2)/\rho_2. \tag{1.1}$$

In this paper we numerically construct a new class of steady, 2-D vortical flows for which there is a balance between the buoyancy force $\mathbf{F}_g$ and the lift force $\mathbf{F}_l$. The fluids are incompressible and inviscid, and the outer fluid is assumed to be irrotational. Within this ''flying droplet'' the vorticity $-\Omega$ is assumed to be a uniform constant; while the droplet boundary may consist of a vortex sheet of net circulation Γ_s. The total circulation of the droplet is then $\Gamma=-a\Omega+\Gamma_s$.

The resulting solutions show several interesting features. In particular, as a function of the Atwood number

$$A=(\rho_1-\rho_2)/(\rho_1+\rho_2),$$

the droplet varies from a circle for $A=0$ to a shape that is approximately a circular cap with two corners at some extreme value $A=A_{\lim}$. We are unable to produce meaningful solutions for $A>A_{\lim}$.

The motivation for considering a steady droplet with constant interior vorticity is partly as a generalization of Prandtl–Batchelor flows, which are flows of a single fluid consisting of regions of constant vorticity surrounded by vortex sheets. Batchelor[1] showed that in region of closed streamlines the inviscid limit of a steady viscous flow must have constant vorticity. Prandtl–Batchelor flows have thus been proposed as the inviscid limit of the wake behind an obstacle. Analytical and computational studies of such flows have been performed in Refs. 2, 5, and 6.

Another context in which such a steady flow could occur is in a rotating flow containing a 2-D droplet (i.e., a 3-D column) of a second fluid of different density (due, for example, to different temperature). In this context the role of gravitational force is played by the centrifugal force. In any such application, the stability of these flows would be important, which has not been considered here.

The formulation and numerical method used here is a boundary integral method and follows closely the method used by Pullin and Grimshaw[2] for computation of interfacial waves. As in their investigation, we are only able to consider droplets with a left-right symmetry. In fact, no well-posed numerical method has been found for asymmetric solutions. They also found extreme solutions consisting of circular caps with singular corners.

In the next section we present Eulerian and Lagrangian formulations of this problem. The Eulerian formulation is easily solved for a small Atwood number as a perturbation expansion; the Lagrangian is most convenient for numerical solution. In particular, we find that the area a and total circulation Γ may be fixed through a rescaling, so that the solution is only a function of the following three parameters: Atwood number $A=(\rho_1-\rho_2)/(\rho_1+\rho_2)$, vorticity value Ω, and the Froude number $\sqrt{c}$. The droplet velocity U is determined through the force balance equation (1.1). A numerical method for solution of this problem is described in the last subsection of Sec. II.

Results from the numerical study are described in Sec. III. In particular, agreement is demonstrated between the numerical solution and the perturbation solution, which serves as a check on their accuracy. Several qualitative properties of

a)Electronic mail: skao@math.cycu.edu.tw
b)Electronic mail: caflisch@math.ucla.edu

the solution, such as the presence of stagnation points, are discussed in Sec. IV in the case of zero interior vorticity ($\Omega=0$) through an additional solution method using conformal mapping. In Sec. V, the angle of the interfaces at the critical Atwood number is shown to be $2\pi/3$ (confirming numerical results in Sec. III). Conclusions from this study are described in Sec. VI.

II. PROBLEM FORMULATION

A. Eulerian formulation

We shall consider the steady state of a two-dimensional inviscid, incompressible droplet of one fluid surrounded by a second fluid under the influence of gravitational acceleration. Assume that there is constant vorticity in the interior and that the droplet boundary is a vortex sheet. Let subscripts 1 and 2 represent fluid properties inside and outside the boundary, respectively, and the gravity acceleration g act in the negative y direction. Denote the density, pressure, and velocity fields by $\rho_i, P_i, \mathbf{u}_i$ for $i=1,2$. The constant values of inner vorticity and vortex sheet circulation are denoted by $-\Omega$ and Γ_s, respectively.

The governing equations in Eulerian coordinates are the following:

$$\rho_i(\mathbf{u}_i\cdot\boldsymbol{\nabla})\mathbf{u}_i+\boldsymbol{\nabla}P_i=-g\rho_i\hat{\mathbf{y}} \quad (x,y)\notin\partial D, \qquad \boldsymbol{\nabla}\cdot\mathbf{u}_i=0, \tag{2.1}$$

$$P_1=P_2 \quad (x,y)\in\partial D, \qquad \mathbf{u}_i\cdot\mathbf{n}=0. \tag{2.2}$$

In (2.1) and (2.2), ∂D is the boundary of the droplet, $\hat{\mathbf{y}}$ is the unit vector in the positive y direction, and $\mathbf{n}$ is the unit normal vector on ∂D. There is a freedom in the position of the center of mass of the droplet, which is fixed by setting it to 0; i.e., $\int_D(x,y)da=(0,0)$.

A particular simple solution of this system with $\rho_1=\rho_2$ is the following:

$$\partial D=\{(x,y):x^2+y^2=1\},$$

$$\mathbf{u}_1=-\frac{r}{2}\,\Omega\,\hat{\boldsymbol{\theta}}, \qquad \mathbf{u}_2=\frac{\Gamma}{2\pi r}\,\hat{\boldsymbol{\theta}}, \tag{2.3}$$

$$P_1=-g\rho_1 y+\frac{\Omega^2}{8}\,\rho_1 r^2-\frac{\Gamma^2}{8\pi^2}\,\rho_1,$$

$$P_2=-g\rho_2 y-\frac{\Gamma^2}{8\pi^2}\,\rho_2\,\frac{1}{r^2}+\frac{\Omega^2}{8}\,\rho_2,$$

in which $\Gamma=-\Omega\pi+\Gamma_s$ is the total circulation, r,θ are variables in the polar coordinates, and $\hat{\mathbf{r}},\hat{\boldsymbol{\theta}}$ are unit vectors. We shall use this as a basic solution from which to construct a perturbation expansion.

When the densities are different, the droplet experiences a buoyancy force $\mathbf{F}_g=-g(\rho_1-\rho_2)\pi\hat{\mathbf{y}}$. We shall allow the flow outside the droplet to move at speed U in the x direction so that the buoyancy force $\mathbf{F}_g$ is balanced through the lift of the Magnus effect, $\mathbf{F}_l=-\Gamma U\rho_2\hat{\mathbf{y}}$. Let the perturbed solution to (2.1), (2.2) for $\rho_1\neq\rho_2$ take the form ($\hat{\mathbf{x}},\hat{\mathbf{z}}$ are unit vectors in the positive x and z directions)

$$\partial D=\{(r,\theta):r=R(\theta)\},$$

$$\mathbf{u}_1=-\frac{r}{2}\,\Omega\,\hat{\boldsymbol{\theta}}+\boldsymbol{\nabla}\times(\psi_1\hat{z})=\boldsymbol{\nabla}\times(\Psi_1\hat{z}),$$

$$\mathbf{u}_2=\frac{\Gamma}{2\pi r}\,\hat{\boldsymbol{\theta}}+U\hat{\mathbf{x}}+\boldsymbol{\nabla}\times(\psi_2\hat{z})=\boldsymbol{\nabla}\times(\Psi_2\hat{z}), \tag{2.4}$$

$$P_1=-g\rho_1 y+\tilde{P}_1,$$

$$P_2=-g\rho_2 y+\tilde{P}_2.$$

In (2.4), Ψ_i is the stream function in fluid i such that $\mathbf{u}_i=(\partial\Psi_i/\partial y),-(\partial\Psi_i/\partial x))$, $i=1,2$. It is given by

$$\Psi_1=\psi_1+\frac{1}{4}\,r^2\Omega, \qquad \Psi_2=\psi_2+Uy-\frac{\Gamma}{2\pi}\log r. \tag{2.5}$$

The Euler equations (2.1) and (2.2) are equivalent to the following form of Bernoulli's law for a fluid without vorticity and one with constant vorticity:

$$\rho_1(\tfrac{1}{2}|u_1|^2-\tfrac{1}{4}r^2\Omega^2-\Omega\psi_1)+\tilde{P}_1=b_1 \quad r<R(\theta), \tag{2.6}$$

$$\nabla^2\psi_1=0, \tag{2.7}$$

$$\rho_2\tfrac{1}{2}|u_2|^2+\tilde{P}_2=b_2 \quad r>R(\theta), \tag{2.8}$$

$$\nabla^2\psi_2=0, \tag{2.9}$$

$$\tilde{P}_1-\tilde{P}_2=g(\rho_1-\rho_2)y \quad r=R(\theta), \tag{2.10}$$

$$\Psi_1=\Psi_2=0. \tag{2.11}$$

Subtracting the two Bernoulli's equations in (2.6), (2.8) on $r=R(\theta)$, and setting $B=b_1-b_2$ (using $\Psi_i=0$ on the boundary), we get

$$\frac{1}{2}\,\rho_1\left\{\left(\psi_{1r}+\frac{R}{2}\,\Omega\right)^2+R^{-2}\psi_{1\theta}^2\right\} -\frac{1}{2}\rho_2\left\{\left(\psi_{2r}-\frac{\Gamma}{2\pi}\,R^{-1}+U\sin\theta\right)^2 +(R^{-1}\psi_{2\theta}+U\cos\theta)^2\right\}+g(\rho_1-\rho_2)y=B. \tag{2.12}$$

Note that Γ,Ω are constants, and that the area and center of the droplet are fixed as

$$\frac{1}{2}\int_0^{2\pi}R^2(\theta)d\theta=\pi, \tag{2.13}$$

$$\int_0^{2\pi}R(\theta)(\cos\theta,\sin\theta)d\theta=(0,0). \tag{2.14}$$

The remaining equations are (2.7), (2.9), (2.11), (2.12), (2.13), and (2.14) for functions ψ_1, ψ_2, R and constants U,B. To solve this system analytically, expand around the special solution at $\rho_1=\rho_2$; i.e.,

$$\begin{aligned}
&\rho_1=\rho_2+\epsilon,\\
&R=1+\epsilon R_1+\epsilon^2 R_2+\cdots\\
&\psi_i=\psi_{i0}+\epsilon\psi_{i1}+\epsilon^2\psi_{i2}+\cdots, \quad i=1,2\\
&U=0+\epsilon U_1+\epsilon^2 U_2+\cdots\\
&B=B_0+\epsilon B_1+\epsilon^2 B_2+\cdots.
\end{aligned} \tag{2.15}$$

The functions ψ_{1j}, ψ_{2j}, and R_j, $j=0,1,2,...$, can be expanded in the angular variable θ, using the equations $\nabla^2\psi_i=0$ for $i=1,2$, as follows:

$$\begin{aligned}
&\psi_{1j}(r,\theta)=\sum_{k=1}^{\infty} a_{jk}r^k\cos k\theta+b_{jk}r^k\sin k\theta,\\
&\psi_{2j}(r,\theta)=\sum_{k=1}^{\infty} c_{jk}r^{-k}\cos k\theta+d_{jk}r^{-k}\sin k\theta,\\
&R_j(\theta)=\sum_{k=1}^{\infty} e_{jk}\cos k\theta+f_{jk}\sin k\theta.
\end{aligned} \tag{2.16}$$

The resulting solution, up to $O(\epsilon^2)$ terms, is

$$\begin{aligned}
&B\simeq\frac{1}{8}\rho_2(\Omega^2-(\Gamma/\pi)^2)+\epsilon\Omega^2/8-\epsilon^2\rho_2 d_1^2,\\
&R(\theta)\simeq 1+\epsilon^2 e_2\cos 2\theta,\\
&\psi_1(r,\theta)\simeq-\Omega/4-\epsilon^2\frac{1}{2}\Omega e_2 r^2\cos 2\theta,\\
&\psi_2(r,\theta)\simeq\epsilon d_1 r^{-1}\sin\theta+\epsilon^2\frac{\Gamma}{2\pi}e_2 r^{-2}\cos 2\theta,\\
&U\simeq-\epsilon d_1,\\
&e_2=4g^2\pi^2\Big/\left\{\left(\Omega^2+\frac{\Gamma^2}{\pi^2}\right)\Gamma^2\rho_2^2\right\} \quad d_1=g\pi/(\Gamma\rho_2).
\end{aligned} \tag{2.17}$$

Thus the shape of the droplet $\partial D=\{(x,y)(\theta)\,|\,0\leqslant\theta<2\pi\}$ is obtained (up to $O(\epsilon^2)$) as

$$x(\theta)=R(\theta)\cos\theta\simeq\left(1+\frac{\epsilon^2}{2}e_2\right)\cos\theta+\frac{\epsilon^2}{2}e_2\cos(3\theta), \tag{2.18}$$

$$y(\theta)=R(\theta)\sin\theta\simeq\left(1-\frac{\epsilon^2}{2}e_2\right)\sin\theta+\frac{\epsilon^2}{2}e_2\sin(3\theta). \tag{2.19}$$

Note that in general the $O(\epsilon)$ term in (x,y) has the form $R_1(\theta)=a\cos\theta+b\sin\theta$. The constraint that the center of mass is 0 implies that this $O(\epsilon)$ term is zero.

B. Lagrangian formulation

We shall work in the complex $z=x+iy$ plane. Describe the boundary of the droplet ∂D by the complex single-valued function $Z(\alpha)=X(\alpha)+iY(\alpha)$, which encloses a connected region D of fluid of constant vorticity $-\Omega$. The parametrization is in the clockwise direction, $0\leqslant\alpha<2\pi$. The velocity field $(u+iv)(z)$ due to the constant vorticity inside the droplet for $z\notin\partial D$ was derived by Pullin in Ref. 6

$$(u-iv)(z)=\frac{\Omega}{4\pi}\oint_{\partial D}\frac{\overline{Z'}-\overline{z}}{Z'-z}\,dZ'. \tag{2.20}$$

For $Z\in\partial D$, we define the velocity $q(Z)=(u+iv)(Z)$ as the average of the limiting values of $(u+iv)(z)$ obtained where $z\to Z(\alpha)$ from either side of ∂D. That is,

$$\begin{aligned}
&q_1(Z)=\lim_{z\to Z \text{ from inside}}(u+iv)(z),\\
&q_2(Z)=\lim_{z\to Z \text{ from outside}}(u+iv)(z),\\
&q(Z)=\tfrac{1}{2}(q_1(Z)+q_2(Z)).
\end{aligned} \tag{2.21}$$

By (2.20) and applying the Plemejl formula, we obtain

$$\overline{q}(Z)=\frac{-\Omega}{4\pi}PV\int_0^{2\pi}\frac{\overline{Z}(\alpha')Z_\alpha(\alpha')d\alpha'}{Z-Z(\alpha')}+\frac{i}{4}\Omega\overline{Z} \qquad Z\in\partial D. \tag{2.22}$$

The velocity field due to the vortex sheet ∂D is given by the Birkhoff–Rott equation

$$\overline{q}(Z)=\frac{1}{2\pi i}PV\int_0^{2\pi}\frac{\gamma(\alpha')d\alpha'}{Z-Z(\alpha')} \quad z\in\partial D \tag{2.23}$$

in which $\gamma(\alpha)=(\overline{q_1}-\overline{q_2})(Z(\alpha))\cdot Z_\alpha(\alpha)$ is the sheet strength with $\int_0^{2\pi}\gamma(\alpha)d\alpha=\Gamma_s$. Combining Eqs. (2.22), (2.23), and taking into account the uniform velocity U at infinity, we have

$$\overline{q}(\alpha)=\frac{1}{2\pi i}PV\int_0^{2\pi}\frac{\gamma'-\Omega i\overline{Z'}Z'_\alpha/2}{Z(\alpha)-Z'}\,d\alpha'+\frac{\Omega i}{4}\overline{Z}(\alpha)+U. \tag{2.24}$$

The quantities with primes in the integral term in (2.24) are functions of the integration variable α'.

To derive the equation for $\gamma(\alpha)$, we use the Bernoulli equations (2.6), (2.8).

$$\frac{1}{2}|u_1|^2+\frac{P_1}{\rho_1}+gy-\Psi_1\Omega=B_1 \quad (x,y) \text{ inside } \partial D, \tag{2.25}$$

$$\frac{1}{2}|u_2|^2+\frac{P_2}{\rho_2}+gy=B_2 \quad (x,y) \text{ outside } \partial D \tag{2.26}$$

in which $B_i=b_i/\rho_i$. By taking Eqs. (2.25) and (2.26) on ∂D and eliminating the pressure terms by the boundary condition $P_1=P_2$, we obtain

$$\gamma\,\mathrm{Re}\left[\frac{q}{Z_\alpha}\right]+A\left(\frac{\gamma^2}{4|Z_\alpha|^2}+\overline{q}q+2gy\right)=B. \tag{2.27}$$

Here $A=(\rho_1-\rho_2)/(\rho_1+\rho_2)$ is the Atwood number, and $B=A(B_1+B_2)+(B_1-B_2)$. The boundary condition $\mathbf{u}_i\cdot\mathbf{n}=0$ yields

$$\mathrm{Im}\left[\frac{q}{Z_\alpha}\right]=0. \tag{2.28}$$

Next we nondimensionalize the problem by setting $Z=L\tilde{Z}$, $\gamma=(L^2/T)\tilde{\gamma}$, $q=(L/T)\tilde{q}$, $U=(L/T)\tilde{U}$, $\Omega=\tilde{\Omega}/T$, $B=(L^2/T^2)\tilde{B}$, $\Gamma=(L^2/T)\tilde{\Gamma}$ and $A=(L/gT^2)\tilde{A}$, where all

variables with ''~'' are the dimensionless quantities. The length scale L is chosen so that the area of the droplet is fixed, as in the Eulerian formulation

$$\int_0^{2\pi} \tilde{y}\, d\tilde{x} = \pi$$

$$\text{or} \qquad \frac{1}{2}\,\mathrm{Im}\left\{ \int_0^{2\pi} \tilde{Z}\overline{\tilde{Z}_\alpha}\, d\alpha \right\} = \pi. \tag{2.29}$$

The time scale T is then chosen so that the total circulation is -1; i.e.,

$$\tilde{\Gamma} = -1. \tag{2.30}$$

Defining $c = L/gT^2$, which equals the square of the Froude number, and dropping ''~'', the resulting nondimensional system is

$$\overline{q}(\alpha) = \frac{1}{2\pi i}\, PV \int_0^{2\pi} \frac{\gamma' - \Omega i \overline{Z'} Z'_\alpha/2}{Z(\alpha) - Z'}\, d\alpha' + \frac{\Omega i}{4}\, \overline{Z}(\alpha) + U, \tag{2.31}$$

$$\gamma\, \mathrm{Re}\left[\frac{q}{Z_\alpha}\right] + A\left(c\left(\frac{\gamma^2}{4|Z_\alpha|^2} + \overline{q}q \right) + 2y \right) = B, \tag{2.32}$$

$$\mathrm{Im}\left[\frac{q}{Z_\alpha}\right] = 0, \tag{2.33}$$

$$\frac{1}{2}\,\mathrm{Im}\left\{ \int_0^{2\pi} Z\overline{Z}_\alpha d\alpha \right\} = \pi, \tag{2.34}$$

$$\int_0^{2\pi} \gamma\, d\alpha' = -1 + \Omega\pi, \tag{2.35}$$

$$\int_0^{2\pi} (\mathrm{Re}(Z(\alpha)), \quad \mathrm{Im}(Z(\alpha)))\, d\alpha = (0,0). \tag{2.36}$$

By Eq. (2.36), the center of the mass of the droplet is always on the origin.

C. Numerical method

The nonlinear system (2.31)–(2.36) in Lagrangian variables is numerically solved by the collocation method. Following Pullin and Grimshaw,[2] we assume that the droplet is symmetric about the imaginary axis $x=0$. We have been unable to find a well-posed numerical method for nonsymmetric shaped droplets. This may be surprising at first, but the same limitation has been found in previous studies of water waves[2] and of Prandtl–Batchelor flows.[5]

The basic unperturbed solution to Eqs. (2.31)–(2.36) for $A=0$ is given by

$$Z(\alpha) = \sin\alpha + i\cos\alpha,$$

$$\gamma(\alpha) = \frac{\Omega}{2} + \frac{\Gamma}{2\pi},$$

$$q(\alpha) = -\frac{\Omega i}{4}\, Z(\alpha) + \frac{\Gamma i}{4\pi \overline{Z(\alpha)}}, \tag{2.37}$$

$$U = 0,$$

$$B = \left(\frac{\Omega}{2} + \frac{\Gamma}{2\pi} \right)\left(\frac{\Omega}{4} - \frac{\Gamma}{4\pi} \right).$$

We shall fix the total circulation by setting $\Gamma = -1$, and express the solution to (2.31)–(2.36) in Fourier expansion around the known solution in (2.37); i.e.,

$$Z(\alpha) = \sin\alpha + i\cos\alpha + X_1 \sin\alpha + i\sum_{j=1}^{N-1} Y_j \cos(j\alpha),$$
$$\gamma(\alpha) = \frac{\Omega}{2} - \frac{1}{2\pi} + \sum_{j=1}^{N-1} C_j \cos(j\alpha). \tag{2.38}$$

Note that our ansatz in (2.38) always satisfies (2.36). Note that omitting the higher wave number sine modes in (2.38) is equivalent to a choice of the parameterization of the boundary curve.

Now insert (2.38) into (2.31)–(2.35). There are $2N+1$ unknowns $\{Y_j, C_j, j=1,2,...,N-1; X_1, B, U\}$. Equation (2.31) serves as a definition of $\overline{q}$, and (2.35) is automatically

TABLE I. Comparison of analytical and numerical results for coefficients X_1, Y_1, Y_2 for various values of Ω and A with $c=1$. The ''error'' here equals max(|analytical X_1-numerical X_1|,|analytical Y_1-numerical Y_1|).

$\Omega=0.0$		numerical		analytical	
A	X_1	Y_1	Y_2	$X_1=-Y_1$	error
0.0025	0.009 715	−0.009 621	0.001 877	0.009 790	1.6876_{-4}
0.0050	0.038 318	−0.036 904	0.013 879	0.039 356	2.4524_{-3}
0.0100	0.147 406	−0.128 469	0.083 501	0.159 019	3.0550_{-2}
0.0200	0.528 120	−0.345 601	0.254 297	0.649 123	3.0352_{-1}
$\Omega=\pm0.5$					
0.0025	0.002 805	−0.002 797	0.000 158	0.002 823	2.6252_{-5}
0.0050	0.011 140	−0.011 018	0.001 217	0.011 350	3.3284_{-4}
0.0100	0.043 404	−0.041 599	0.008 504	0.045 861	4.2623_{-3}
0.0200	0.164 832	−0.141 507	0.046 575	0.187 207	4.5700_{-2}
$\Omega=\pm1.0$					
0.0025	0.000 896	−0.000 895	0.000 016	0.000 901	5.7912_{-6}
0.0050	0.003 574	−0.003 561	0.000 128	0.003 621	5.9830_{-5}
0.0100	0.014 148	−0.013 951	0.000 967	0.014 630	6.7906_{-4}
0.0200	0.054 722	−0.051 883	0.006 468	0.059 719	7.8363_{-3}
0.0400	0.209 660	−0.173 321	0.033 411	0.248 933	7.5612_{-2}
$\Omega=\pm1.5$					
0.0025	0.000 420	−0.000 419	0.000 004	0.000 422	2.3925_{-6}
0.0050	0.001 677	−0.001 674	0.000 028	0.001 696	2.2183_{-5}
0.0100	0.006 672	−0.006 628	0.000 219	0.006 852	2.2443_{-4}
0.0200	0.026 193	−0.025 524	0.001 588	0.027 971	2.4471_{-3}
0.0400	0.099 902	−0.090 828	0.009 499	0.116 596	2.5768_{-2}
0.0800	0.428 225	−0.299 830	0.045 280	0.507 823	2.0799_{-1}

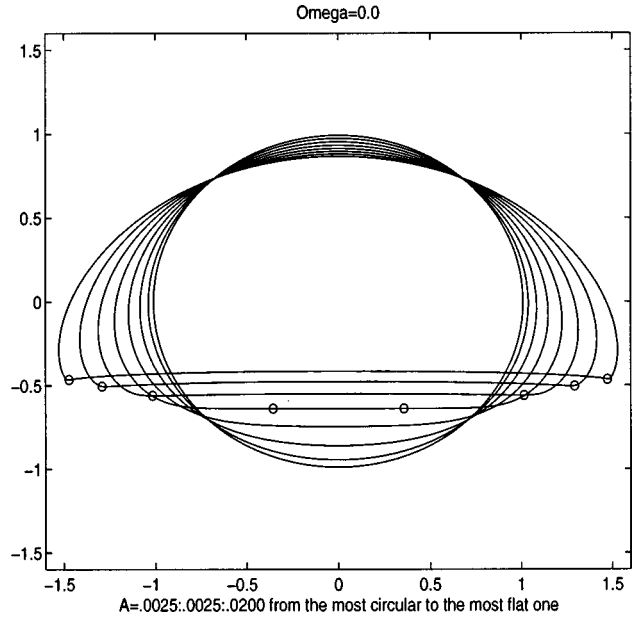

FIG. 1. The stationary profiles of the droplet at $\Omega=0.0$ at various A.

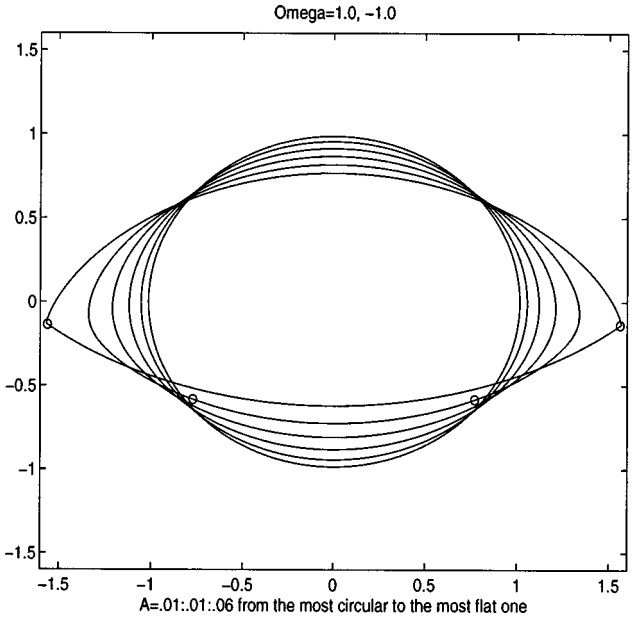

FIG. 3. The stationary profiles of the droplet at $\Omega=\pm 1.0$ at various A.

satisfied. Evaluating (2.32), (2.33) at N points $\alpha_{k-1/2}=(k-\frac{1}{2})\pi/N$ for $k=1,2,...,N$, plus (2.34), results in a total of $2N+1$ equations. The principal-valued integral in (2.31) is evaluated by summing over $\alpha_j'=j(\pi/N)$, $j=1,2,...,2N$, for each $\alpha_{k-1/2}$. Newton's iterative scheme is used to solve this closed $2N+1$ linear system, and the iteration stops when the absolute value of the difference between two successive iterative solutions is less then 10^{-7}. The initial guess for the Newton iteration was generated by a continuation method. For $A=0$, the solution is just the simple circular droplet described above. Once a solution was computer for $\tilde{A}$, that solution is used as an initial guess for the computation at $A=\tilde{A}+\delta A$. If the iteration fails to converge, then the increment in the Atwood number, δA, was halved, until δA was as small as $10^{-2}/2^8$. This allowed us to perform computation almost up to the critical value $A_{\lim}$.

The problem was solved for various values of A and Ω, and for a typical value of $N=128$. We check that the computation provides consistent solutions to the nonlinear system by showing the numerical solutions converge as the mesh size shrinks. Since Newton's iterative scheme converges quadratically, it takes usually three to four iterations to reach the 10^{-7} error bound.

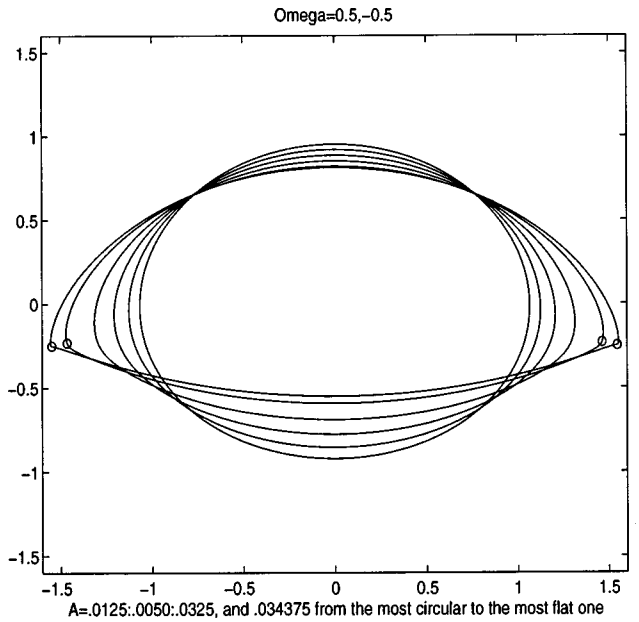

FIG. 2. The stationary profiles of the droplet at $\Omega=\pm 0.5$ at various A.

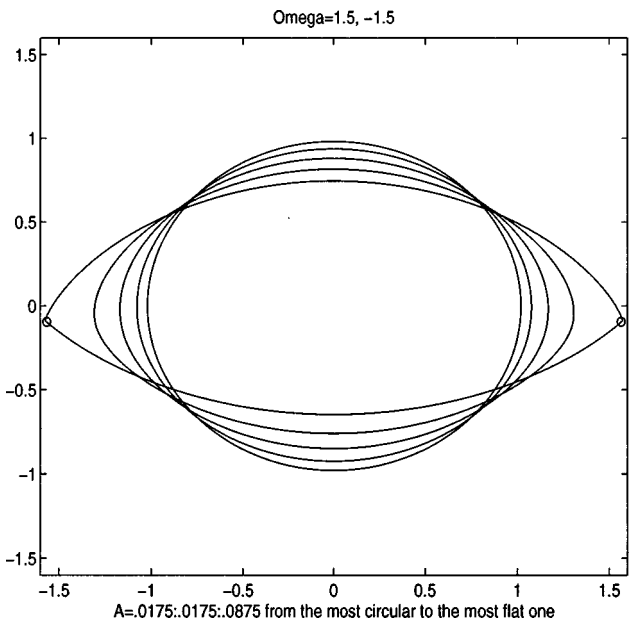

FIG. 4. The stationary profiles of the droplet at $\Omega=\pm 1.5$ at various A.

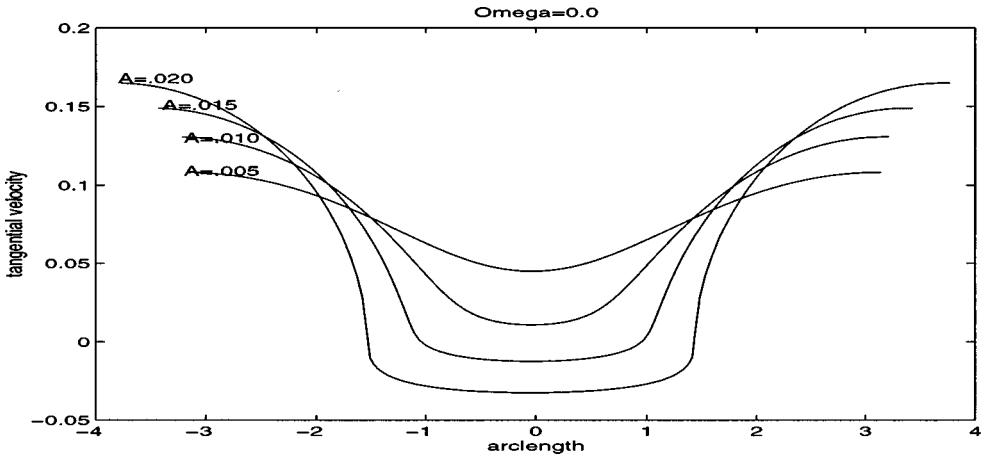

FIG. 5. The tangential velocity vs arclength of ∂D at $\Omega=0.0$ for $A=0.005$, 0.010, 0.015, 0.02. The bottom of the droplet corresponds to zero arclength, and the sign of arclength changes from negative to positive clockwise along ∂D.

III. RESULTS

A. Agreement between the Eulerian and Lagrangian formulations

To demonstrate the validity of both the analytic and numerical results, we perform a comparison of the (analytical) Eulerian and (numerical) Lagrangian solutions. In order to make this comparison, we first cast the analytical solution into Lagrangian form. Since the parameters θ in the Eulerian formulation, and α in the Lagrangian formulation are different, we must first establish their relationship. The boundary of the droplet ∂D is described by two parameterizations: $\{(x,y)(\theta)|0\leqslant\theta<2\pi\}$ for the Eulerian and $\{(X,Y)(\alpha)|0\leqslant\alpha<2\pi\}$ for the Lagrangian formulation, where

$$x(\theta)=\cos\,\theta+\sum_{k\geqslant 1} a_k\cos(k\theta), \tag{3.39}$$

$$y(\theta)=\sin\,\theta+\sum_{k\geqslant 1} b_k\sin(k\theta), \tag{3.40}$$

$$X(\alpha)=\sin\,\alpha+X_1\sin\,\alpha, \tag{3.41}$$

$$Y(\alpha)=\cos\,\alpha+\sum_{k\geqslant 1} Y_k\cos(k\alpha). \tag{3.42}$$

The relations among the coefficients X_1, a_k, Y_k, and b_k for $k\geqslant 1$ are derived by setting

$$(x,y)(\theta)=(X,Y)(\alpha). \tag{3.43}$$

In the particular solution with $\rho_1=\rho_2$ $(\epsilon=0)$, the parameters are related by

$$\alpha=\frac{\pi}{2}-\theta. \tag{3.44}$$

Thus for $\rho_1\neq\rho_2$ we can assume that

$$\alpha=\frac{\pi}{2}-\theta+\epsilon f_1(\theta)+\epsilon^2 f_2(\theta)+\cdots. \tag{3.45}$$

Replacing α in (3.41), (3.42), by (3.45), and using the solutions derived in (2.18), (2.19) leads to

$$f_1=0,$$

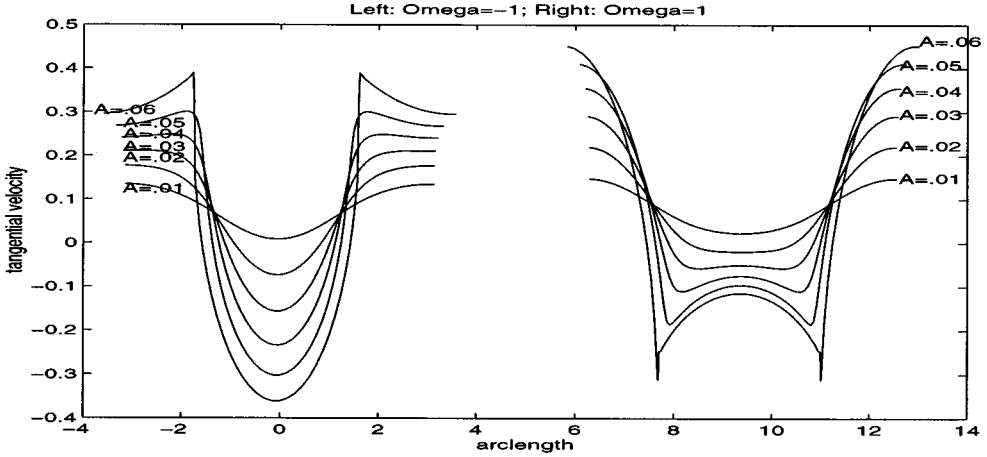

FIG. 6. The tangential velocity vs arclength of ∂D at $\Omega=\pm 1$ for $A=0.01{:}0.01{:}0.06$. The bottom of the droplet corresponds to zero arclength, as in Fig. 5. The arclength for the plot for $\Omega=1$ is shifted by 3π.

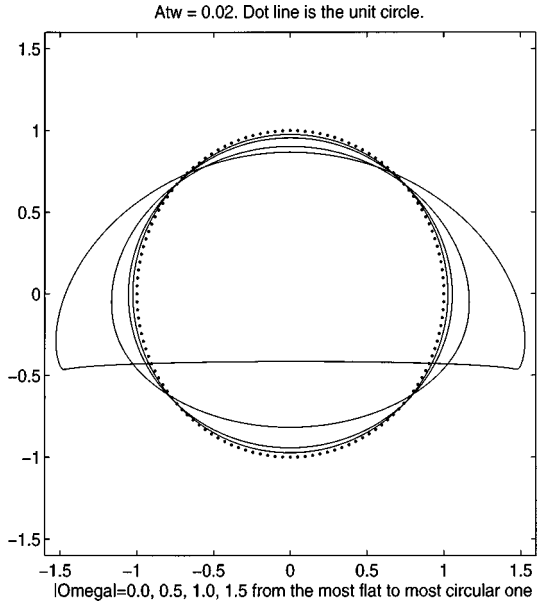

FIG. 7. Stationary shapes for various $|\Omega|$ at $A=0.02$.

$$f_2=-2e_2 \sin\theta \cos\theta,$$
$$X_1=-Y_1=\epsilon^2 e_2, \tag{3.46}$$
$$Y_2=O(\epsilon^3).$$

Next, note that the nondimensional form of Eq. (2.12) is the same except that g is replaced by $gT^2/L=c^{-1}$. By choosing $c=1$, the asymptotic solution obtained in Section 2.1 is nondimensionalized by setting $g=1$. To relate $\epsilon=\rho_1-\rho_2$ and the Atwood number A, we nondimensionalize ϵ as $\tilde{\epsilon}=\epsilon/\rho_2=(\rho_1-\rho_2)/\rho_2=2A/(1-A)$.

Using these values, we compare the results of the analytical and numerical solutions. In Table I, there is a comparison of the values of X_1, Y_1, Y_2 for the analytical [with error $O(A^3)$] and numerical solutions for a range of values of A and Ω, showing excellent agreement. We have also compared the numerically computed velocity U with the exact analytical result $U=-\epsilon d_1$, and obtained agreement to all significant precision.

B. Discussion

Here we present the stationary profiles of the droplet and the corresponding velocity fields derived by our numerical results. In Figs. 1 to 4, we plot the shape of the droplet at various A up to A_{lim}, beyond which the iteration scheme fails to converge, for $\Omega=0.0$, ± 0.5, ± 1.0, and ± 1.5, and the circles mark the stagnation points. The tangential velocity for $\Omega=0$, ± 1 for some chosen A's is shown in Figs. 5 and 6.

These results show that the stationary shape of the droplet is nearly independent of the sign of Ω, but the direction of the interior velocity field changes sign as Ω changes sign. This is consistent with (2.17), which shows that the leading order terms in the shape of the droplet depend on Ω^2. On the other hand, the leading order term for the interior velocity is proportional to Ω.

Larger values of $|\Omega|$ result in larger A_{lim}'s, which means that the vorticity supports the boundary and hence the droplet is less deformed at the same A, as shown in Fig. 7. Examination of the tangential velocity shows that the two corners on the profiles at $A=A_{\text{lim}}$ are stagnation points.

Stagnation points (and stagnation streamlines emanating from the stagnation points) determine the geometric character of the flow. For $A=0$ (i.e., $\rho_1=\rho_2$) the flow is purely rotating without stagnation points. For the special case $\Omega=0$, the analysis of the next section and the numerical results of Fig. 5 show the A dependence of the stagnation points. For small A, there is a single stagnation point in the exterior flow. At a particular value of A, this stagnation points hits the droplet boundary. For larger A values it splits into two stagnation points on the boundary, which are at the droplet corners at the critical values of A.

For nonzero Ω, the determination of the stagnation points is less complete, since there are no exact analytic re-

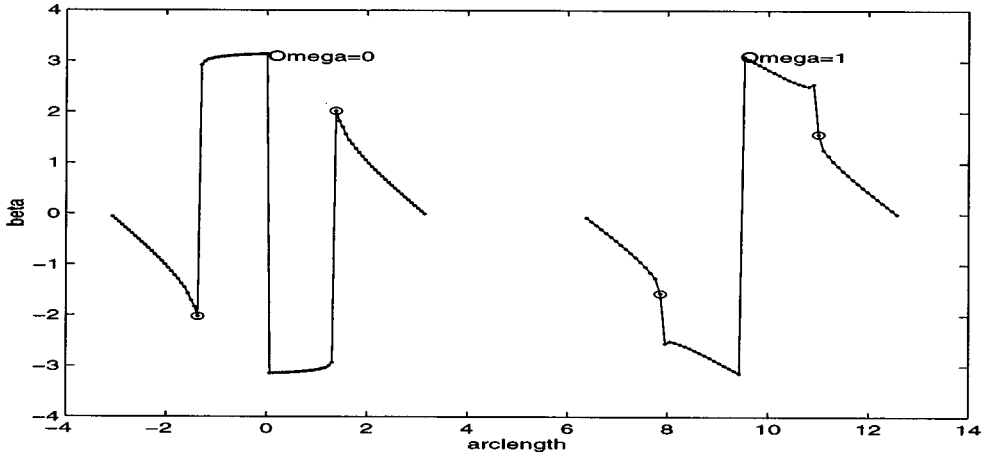

FIG. 8. The angle between the tangential vector along ∂D and the positive x-axis vs. arclength for $\Omega=0$, $\Omega=1$. As in Fig. 5, the bottom of the droplet corresponds to zero arclength. The arclength for the plot for $\Omega=1$ is shifted by 3π.

TABLE II. Angle of the stagnation points at $A=A_{\rm lim}$ from numerical results for various cases.

	Angle for $c=1$			
	$N=64$	$N=96$	$N=128$	$N=256$
$\Omega=0$ ($A_{\rm lim}=2.000_{-2}$)	-	1.7366	2.1410	2.0833
$\lvert\Omega\rvert=0.5$ ($A_{\rm lim}=3.438_{-2}$)	1.8710		2.0491	2.1305
$\lvert\Omega\rvert=1.0$ ($A_{\rm lim}=6.000_{-2}$)	2.1096		2.0929	2.1233
$\lvert\Omega\rvert=1.5$ ($A_{\rm lim}=8.750_{-2}$)	1.9891		2.0934	⋯
	Angle for $\Omega=0$			
	$N=96$		$N=128$	$N=256$
$c=1$ ($A_{\rm lim}=2.000_{-2}$)	1.7366		2.1410	2.0833
$c=16$ ($A_{\rm lim}=1.500_{-2}$)	1.9735		1.9249	2.0245
$c=32$ ($A_{\rm lim}=1.266_{-2}$)	1.9936		2.1029	⋯
$c=48$ ($A_{\rm lim}=1.000_{-2}$)	1.9829		2.1285	2.0983

sults available. The numerical results of Fig. 6, however, show the same type of behavior of nonzero Ω as in the $\Omega=0$ case.

Figure 8 shows the angle between the tangential vector along ∂D and the positive x axis, denoted by β, at $A=A_{\rm lim}$ for $\Omega=0$ and $\Omega=1$. The sharp jump of β on the corners of the boundary indicates the existence of the singularity (the larger jump in the center of the curve is a resetting of the angle by 2π). the angle jumps from negative to positive for $\Omega=0$, and from negative to negative (or positive to positive) for $\Omega\neq 0$, corresponds to the difference between the mushroom-cap solution of Fig. 1 and the lozenge shape of Fig. 3. The corner angle is analytically shown to be $2\pi/3\simeq 2.0944$ in Sec. V for all Ω and c. Computations of the angle for a number of values of Ω and c are presented in Table II, showing excellent agreement (4% accuracy in all cases) with the analytic result.

Finally, the dependence of the solution on the Froude number $\sqrt{c}$ is very mild. Figure 9 for $\Omega=0$, $A=0.01$ shows a typical example. The solutions for c close to 1 (including $c\to 0$) are all almost identical. Only for large variations in c (~ 30) are there corresponding changes in the droplet shape.

Additional features of the flow are presented in Figs. 10–18, which plot the exterior velocity field at various parameter values. The vorticity density on the droplet boundary is plotted in Fig. 19. There is a pair of points where the sheet strength γ is not differentiable. They correspond to the corner points of the corresponding limiting profiles. These are same points at which the tangential velocity is nondifferentiable, as seen in Figs. 5 and 6.

These results bear similarity to the results of Pullin and Grimshaw[2] for nonlinear interfacial gravity waves in a two-layer Boussinesq fluid, in which the upper layer consists of a flow of constant vorticity and the lower layer is irrotational. They found that the most extreme wave was consistent with the appearance of one or more stagnation points on the wave profile. The result that the droplet boundary is less deformed for larger values of the interior vorticity was also found by Moore, Saffman, and Tanveer[5] when they studied the Batchelor flows in the cases of the Sadovskii vortex and the rotational corner flow. The semicircular shape of the solution for $\Omega=0.0$ at $A_{\rm lim}$ also resembles the cap of the ''mushroom'' solution in the steady wave problem found by Pullin and Grimshaw.[3,4]

IV. SOLUTION FOR $\Omega=0$

Here we present additional analysis of the ''flying droplet'' problem in the special case $\Omega=0$; i.e., for irrotational flow inside the droplet. In this case, the problem can be conveniently formulated as conformal mapping problem. Using this formulation, several qualitative properties of the solution are easily obtained: First, for $\Omega=0$ the solution is independent of the parameter c. Second, the flow has three possible forms with either a single stagnation point in the exterior flow, a single stagnation point on the droplet boundary, or two stagnation points on the boundary.

A. Conformal mapping formulation for $\Omega=0$

If $\Omega=0$, the droplet problem can be written in Eulerian variables as the following equation for the potentials ϕ_1 and ϕ_2 inside and outside of D, respectively,

$$\nabla^2\phi_1=0 \quad \text{inside } D,$$
$$\nabla^2\phi_2=0 \quad \text{outside } D, \tag{4.1}$$

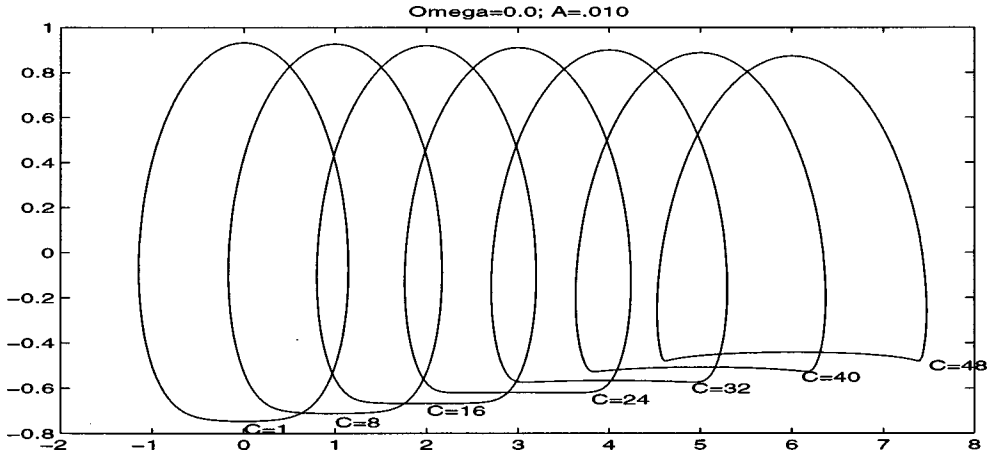

FIG. 9. The stationary shape for $\Omega=0.0$, $A=0.010$ at various c. Only the most left profile is at the correct x coordinate, while the other profiles are successively shifted by 1.0 unit in the positive x direction.

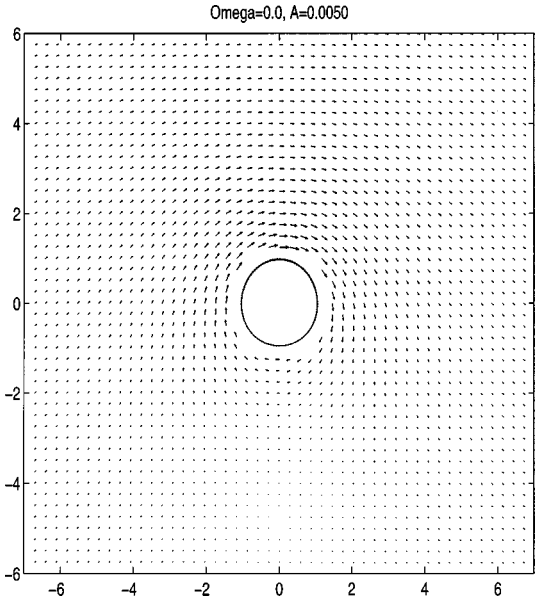

FIG. 10. The velocity field for $\Omega=0$, $A=0.0050$.

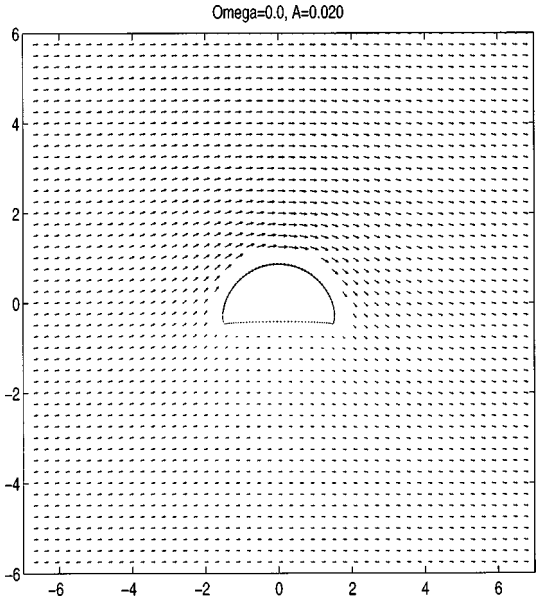

FIG. 12. The velocity field for $\Omega=0$, $A=0.020$.

with

$$\mathbf{n}\cdot\nabla\phi_1=\mathbf{n}\cdot\nabla\phi_2=0,$$

$$\rho_1\tfrac{1}{2}|\nabla\phi_1|^2+p_1=-\rho_1 gy+b_1,$$

$$\rho_2\tfrac{1}{2}|\nabla\phi_2|^2+p_2=-\rho_2 gy+b_2, \tag{4.2}$$

on the boundary of D and with

$$\phi_2\to(2\pi)^{-1}\Gamma\theta-\mathbf{w}\cdot\mathbf{x} \tag{4.3}$$

as $|\mathbf{x}|\to\infty$.

The solution inside the droplet is

$$\phi_1=0,$$

$$p_1=-\rho_1 gy+b_1, \tag{4.4}$$

so that the equations for $\phi=\phi_2$ become

$$\nabla^2\phi=0 \quad \text{in } D^c$$

$$n\cdot\nabla\phi=0 \quad \text{on } \partial D$$

$$|\nabla\phi|^2=2g\epsilon y+b \quad \text{on } \partial D$$

$$\phi\to(2\pi)^{-1}\Gamma\theta-\mathbf{w}\cdot\mathbf{x} \quad \text{as } |\mathbf{x}|\to\infty \tag{4.5}$$

in which ϵ is the nondimensionalized density parameter from Sec. II A,

$$\epsilon=2A/(1-A)=\frac{\rho_1-\rho_2}{\rho_2}. \tag{4.6}$$

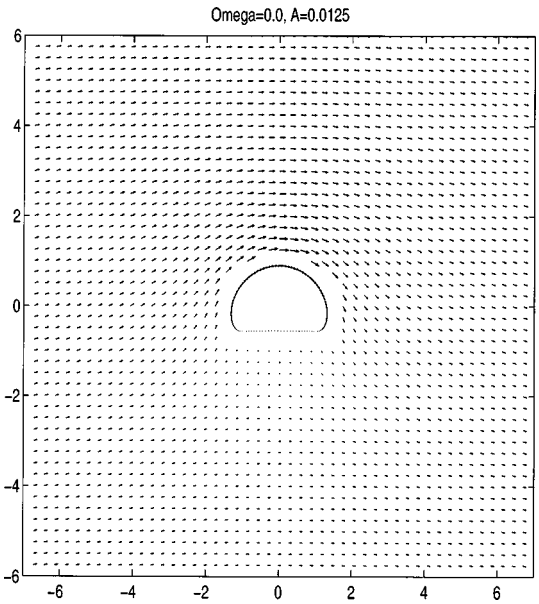

FIG. 11. The velocity field for $\Omega=0$, $A=0.0125$.

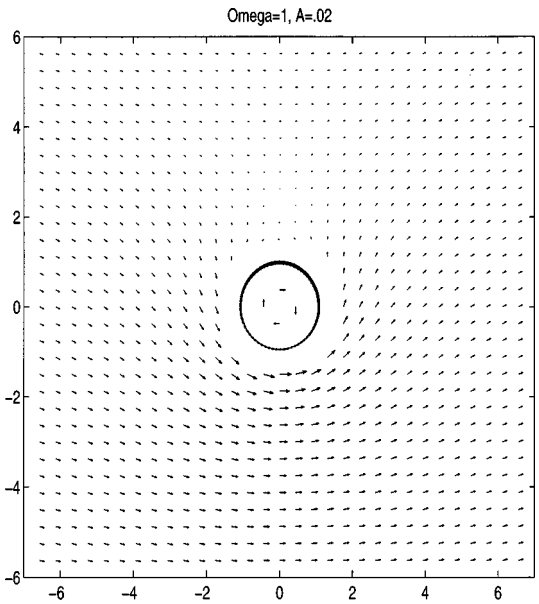

FIG. 13. The velocity field for $\Omega=1$, $A=0.02$.

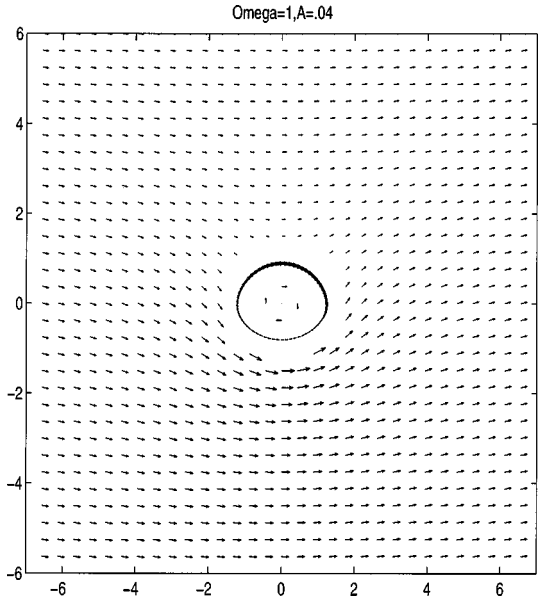

FIG. 14. The velocity field for $\Omega=1$, $A=0.04$.

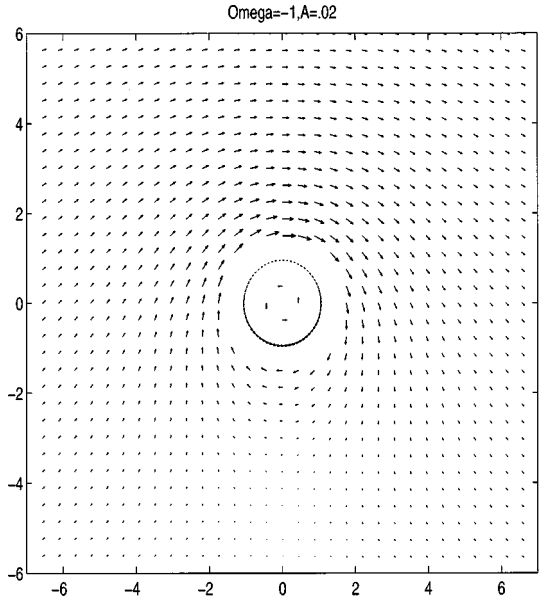

FIG. 16. The velocity field for $\Omega=-1$, $A=0.02$.

Define the area of D as a; the Jakowski lift theorem then says that

$$\mathbf{w}=(U,0),$$

$$U\Gamma\rho_2=-g(\rho_1-\rho_2)a, \tag{4.7}$$

as in (1.1)

This problem can be rewritten using a conformal mapping $z(\zeta)=x+iy$ taking the exterior of the unit circle $|\zeta|>1$ to the exterior of D. For a given shape D, this conformal map is fixed by requiring that real direction in ζ goes to the real direction in z at infinity, i.e.,

$$z=z_0\zeta \quad \text{as } |\zeta|\to\infty. \tag{4.8}$$

in which the real parameter z_0 must be determined. Set $\zeta=re^{i\alpha}$. Then the equations for ϕ are

$$\nabla^2\phi=0 \quad r>1, \tag{4.9}$$

$$\phi_r=0 \quad r=1, \tag{4.10}$$

$$\phi_\alpha^2=(2g\epsilon y+b)(y_r^2+y_\alpha^2) \quad r=1, \tag{4.11}$$

$$\phi\to(2\pi)^{-1}\Gamma\alpha+ruz_0\cos\alpha \quad r\to\infty. \tag{4.12}$$

The solution of (4.9), (4.10), (4.12) is

$$\phi=(2\pi)^{-1}\Gamma\alpha-(r+r^{-1})u\cos\alpha z_0. \tag{4.13}$$

Equation (4.11) then becomes part of the equations for y which are

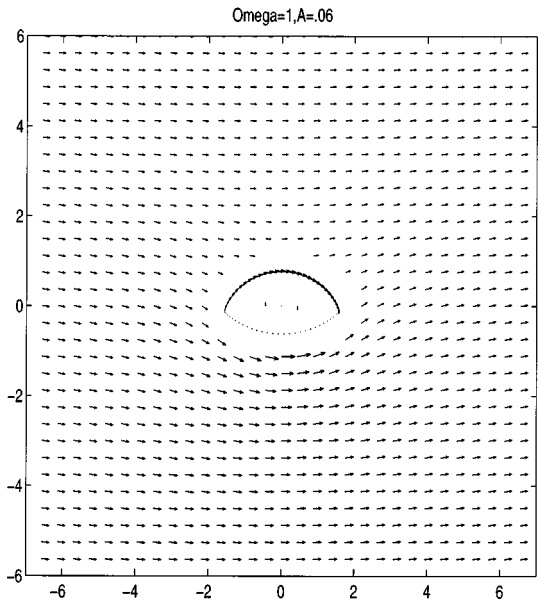

FIG. 15. The velocity field for $\Omega=1$, $A=0.06$.

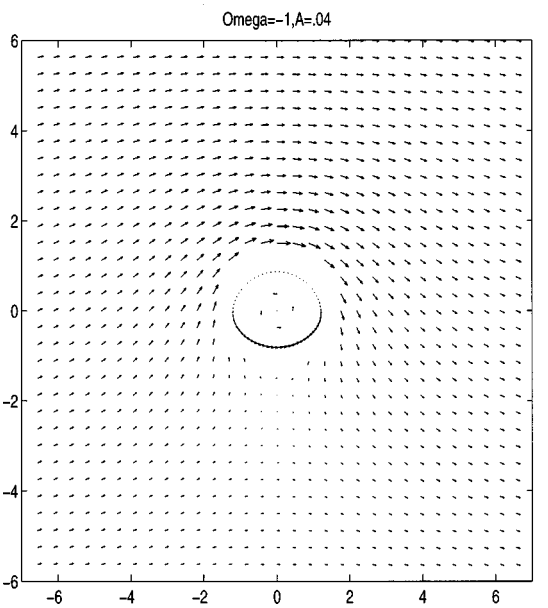

FIG. 17. The velocity field for $\Omega=-1$, $A=0.04$.

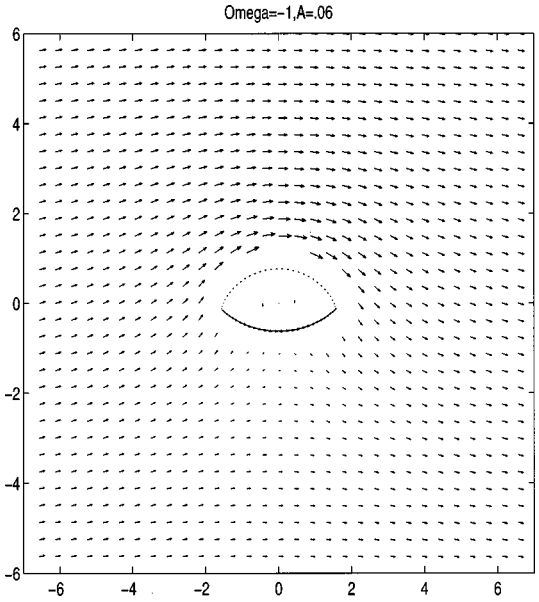

FIG. 18. The velocity field for $\Omega=-1$, $A=0.06$.

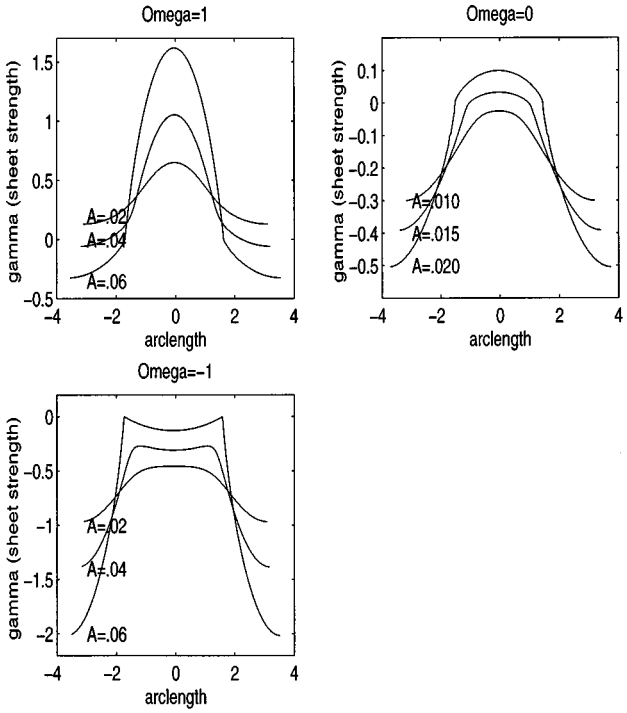

FIG. 19. The vorticity density vs arclength for different Ω's.

$$\nabla^2 y=0, \quad r>1,$$

$$(2g\epsilon y+b)(y_r^2+y_\alpha^2)=((2\pi)^{-1}\Gamma+2uz_0\sin\alpha)^2 \quad r=1,$$

$$y\to z_0 r\sin\alpha, \quad r\to\infty.$$

In addition x can be solved using the Cauchy–Riemann equations

$$x_r=y_\alpha, \tag{4.14}$$

$$x_\alpha=-y_r. \tag{4.15}$$

Now nondimensionalize the conformal mapping problem as

$$y=Ly', \quad z_0=Lz_0',$$

$$u=(L/t)u', \quad b=(L^2/T^2)b',$$

$$g=(L/t^2)g', \quad \epsilon=g'^{-1}\epsilon',$$

$$\Gamma=(L^2/T)\Gamma', \quad a=La', \tag{4.16}$$

in which

$$\Gamma'=1, \quad u'=\pi\epsilon'.$$

Then (4.7) implies that the nondimensionalized area is

$$a'=\pi$$

and in the dimensionless variables the conformal mapping equation becomes (dropping primes)

$$\nabla^2 y=0 \quad r>1,$$

$$(2\epsilon y+b)(y_r^2+y_\alpha^2)=((2\pi)^{-1}+2\pi\epsilon z_0\sin\alpha)^2 \quad r=1,$$

$$y\to z_0 r\sin\alpha \quad r\to\infty. \tag{4.17}$$

Note that in this formulation the parameter c (squared Froude number) does not appear, since the gravitational constant g has been removed through the nondimensionalization of ϵ. Thus in the case $\Omega=0$, the solution does not depend on c. This can also been seen directly from the Lagrangian formulation of Sec. II using the variable $q=q_2+(\gamma/2z_\theta)$.

B. Stagnation points

In conformal mapping formulation, one can easily characterize the stagnation points of the flow. They are points at which $\nabla\phi=0$ for $r>1$ (in the outer fluid) or $|\nabla\phi|=|\phi_\alpha|=0$ for $r=1$ (on the boundary).

In dimensionless variables

$$\phi=(2\pi)^{-1}\alpha-\pi\epsilon z_0(r+r^{-1})\cos\alpha \tag{4.18}$$

with

$$\phi_r=-\pi\epsilon z_0(1-r^{-2})\cos\alpha,$$

$$\phi_\alpha=(2\pi)^{-1}+\pi\epsilon z_0(r+r^{-1})\sin\alpha, \tag{4.19}$$

and for $r=1$

$$|\nabla\phi|^2=\phi_\alpha^2=(2\pi\epsilon z_0\sin\alpha+(2\pi)^{-1})^2. \tag{4.20}$$

Thus we get the following characterization:

(i) For $\epsilon z_0<(2\pi)^{-2}$ there is exactly 1 stagnation point at $\alpha=-\pi/2$, $(r+r^{-1})=(2\pi^2\epsilon z_0)^{-1}$ which is in the exterior flow.

(ii) For $\epsilon z_0=(2\pi)^{-2}$ there is 1 stagnation point on $r=1$ at $\alpha=-\pi/2$, which is the bottom of the droplet.

(iii) For $\epsilon z_0>(2\pi)^{-2}$ there are exactly 2 stagnation points on $r=1$.

V. INTERIOR ANGLE OF THE DROPLET FOR CRITICAL *A*

When a corner develops in the boundary of the droplet, as observed at the critical Atwood number, the interior angle

of the droplet and the angle of the droplet with the exterior stagnation streamline is exactly $2\pi/3$. Numerical results showing this result were presented in Table II and discussed in Sec. III. An analytic proof is presented here; it is a modification of the proof for the angle of Stokes wave of greatest height.

For $\Omega=0$ the argument for angle $2\pi/3$ is exactly the same as the Stokes argument, since the pressure inside the droplet is constant, as in the water wave problem.

For $\Omega\neq 0$ the pressure is not constant and may bring in its own singularities. So a different argument is required: Suppose that the pressure P_i and the perturbation streamfunction ψ_i contain fractional powers at $x=0$, the stagnation point. Since ψ_1 and ψ_2 are harmonic, then

$$\psi_1=\mathrm{Imag}(c_1 z^{m_1}),$$

$$\psi_2=\mathrm{Imag}(c_2 z^{m_2}).$$

We wish to show that $m_1=m_2=3/2$. Assuming that $m_i<2$, then the dominant terms in the Bernoulli equations (2.6) and (2.8) are $\rho_i|u_i|^2$ and $\tilde{P}_i$. This implies that $\tilde{P}_i\approx b_i|z|^{2m_i-2}$. The pressure jump condition (2.10) then implies that $m_1=m_2$. Assume that there is a single stagnation streamline in the exterior region, then (2.11) says that ψ_i is smooth on the three streamlines (one stagnation streamline and the two branches of the bubble boundary). This implies that $m_i=3/2$.

VI. CONCLUSIONS

The solutions found above represent a new class of steady flows for a droplet in an inviscid, incompressible 2-D fluid. In these flows there is a balance between the buoyancy force due to gravity and the lift force due to circulation and translation. These flows are of Prandtl–Batchelor type in that the vorticity is constant in regions of closed streamlines. After nondimensionalization, the solution is found to depend on three parameters: the Atwood number A, the interior vorticity $-\Omega$, and Froude number $\sqrt{c}$. When $A=0$ the solution is just a circular droplet with purely rotating flow. For the simple case $\Omega=0$, the solution does not depend on the parameter c.

As the Atwood number A increases (or decreases) from 0, the droplet boundary remains smooth until a critical value of A is reached at which the boundary develops two corners. The angle of this corner is $2\pi/3$, according to a modification of the Stokes wave angle argument.

Only symmetric solutions have been investigated here. As pointed out in Ref. 3, nonsymmetric solutions could possibly appear through bifurcation off solution branches of symmetric shapes.

Stability of these flows would be important for any application but has not been investigated, since it is outside the scope of the present work. Nonzero vortex sheet strength on the droplet boundary should make the problem strongly unstable. On the other hand, the overall rotation may help stabilize the flow.

ACKNOWLEDGMENTS

S.-S.K. acknowledges support by NSC Grant No. 86-2115-M-033-001. R.E.C. acknowledges support by DARPA under URI Grant No. N00014092-J-1890. We are happy to acknowledge the motivation and technical help that we received through numerous discussions with Huaxiong Huang, Qing Nie, Derek Moore, and Dale Pullin. We also thank two anonymous referees who suggested numerous improvements in the paper.

[1] G. K. Batchelor, ''A proposal concerning laminar wakes behind bluff bodies at large Reynolds number,'' J. Fluid Mech. **1**, 388 (1956).
[2] R. H. J. Grimshaw and D. I. Pullin, ''Interfacial progressive gravity waves in a two-layer shear flow,'' Phys. Fluids **26**, 1731 (1983).
[3] R. H. J. Grimshaw and D. I. Pullin, ''Extreme interfacial waves,'' Phys. Fluids **29**, 2802 (1986).
[4] R. H. J. Grimshaw and D. I. Pullin, ''Finite-amplitude solitary waves at the interface between two homogeneous fluids,'' Phys. Fluids **31**, 3550 (1988).
[5] D. W. Moore, P. G. Saffman, and S. Tanveer, ''The calculation of some Batchelor Flows: the Sadovskii vortex and rotational corner flow,'' Phys. Fluids **31**, 978 (1988).
[6] D. I. Pullin, ''The nonlinear behavior of a constant vorticity layer at a wall,'' J. Fluid Mech. **108**, 401 (1981).